IFUP–TH/2005–36
GEF-TH-2005-11

Behaviour of the topological susceptibility in two colour QCD across the finite density transition

B. Allés[a], M. D'Elia[b], M. P. Lombardo[c]

[a] *INFN, Sezione di Pisa, Pisa, Italy*

[b] *Dipartimento di Fisica, Università di Genova and INFN, Genova, Italy*

[c] *INFN, Laboratori Nazionali di Frascati, Frascati, Italy*

Abstract

The behaviour of the topological susceptibility χ in QCD with two colours and 8 flavours of quarks is studied at nonzero temperature on the lattice across the finite density transition. It is shown that the signal of χ drops abruptly at a critical chemical potential μ_c, much as it happens at the finite temperature and zero density transition. The Polyakov loop and the chiral condensate undergo their transitions at the same critical value μ_c. At a value μ_s of the chemical potential, called saturation point, which in our case satisfies $\mu_s > \mu_c$, Pauli blocking supervenes and consequently the theory becomes quenched.

I. INTRODUCTION

The topological susceptibility χ has many applications in QCD. It is defined as the correlation function of two topological charge density operators $Q(x)$ at zero momentum where $Q(x)$ is

$$Q(x) = \frac{g^2}{32\pi^2}\epsilon_{\zeta\nu\gamma\sigma}F^a_{\zeta\nu}(x)F^a_{\gamma\sigma}(x)\,, \tag{1.1}$$

and $F^a_{\zeta\nu}(x)$ is the gluon tensor. The quenched value of χ is responsible for the large mass of the η' meson [1,2] and allows to understand the realization of the $\mathrm{U_A}(1)$ symmetry. From phenomenology this quantity must be $\chi \approx (180\ \mathrm{MeV})^4$. The most recent lattice results [3–5] and calculations based on SVZ–sum rules [6] are in fair agreement with this prediction. Besides, in the full theory χ is proportional to the chiral condensate in the massless limit [7] while the second moment of the correlation function of two topological charge density operators furnishes a possible explanation to the so–called proton spin crisis [8].

The behaviour of the topological susceptibility at finite temperature and/or matter density is an important ingredient to understand whether or not the singlet chiral symmetry undergoes some sort of effective restoration at extreme conditions. The fate of this symmetry and of the non–singlet chiral symmetry and the ordering of the respective phase transitions open several scenarios [9–12] with relevant physically measurable consequences.

It is known that χ undergoes an abrupt drop at the deconfinement transition at finite temperature in Yang–Mills theory, both for two [13] and three [14] colours, and in full QCD for three colours and 2 or 4 flavours of staggered quarks [15]. These results have been confirmed by many collaborations by using cooling [3,16,17]* (see however [18]) and by counting fermionic zero modes [19], including studies for $N \geq 4$ colours.

---

*Older papers claimed that the signal dissapeared smoothly and it began to fade away well before the deconfinement temperature; however nowadays this possibility seems excluded.

In this paper we present an investigation about the behaviour of χ at finite temperature and density. This study has been carried out considering two colour QCD. In this case we do not have to face the hard sign problem of numerical simulations in three colour QCD at finite density (although several techniques to overcome these difficulties have been proposed [20–22]).

Several analyses of two colour QCD at finite density are available in the literature [23–31] and one expects that the qualitative aspects of the behaviour of gluonic observables can be extended to three colour QCD. In particular, for the topological susceptibility, this expectation is further supported by the fact that instantons [32] are present in any SU(N) gauge group theory. Monte Carlo results bear out this expectation both for the validity of the Witten–Veneziano mechanism as well as for the sudden drop of the signal of χ at the deconfinement transition [3,13,17].

Model studies suggest that instantons form structures with different features as the temperature and density change [33,34]. Beyond the finite density transition instantons seem to cluster into polymers while at the deconfinement temperature and zero density they tend to form instanton–antiinstanton pairs.

We have investigated the behaviour of χ on the lattice as the density of matter is varied at finite temperature. The temperature was introduced as usual by compactifying the temporal direction of the lattice and the density by switching on a chemical potential μ for quarks. Fermions have been discretized by using the staggered formulation [35]

The two main results of our numerical study are: *i)* the topological susceptibility drops at a critical μ_c and *ii)* this μ_c is the same value of the chemical potential where the chiral condensate falls and the Polyakov loop rises. Moreover the introduction of a density of matter brings forth the following effect. The density of fermions grows as the value of μ is increased up to a saturation point, $\mu_s > \mu_c$, where no more fermions can be inserted into the system. In fact, due to the Pauli exclusion principle, there cannot be more than $N_f/4$ fermions per site for SU(2) gauge group and N_f flavours (which in our case is equivalent to $N_f/8$ baryons per site). This number follows from the fact that in the staggered formulation, one Dirac

spinor is reconstructed from the fields at the 16 sites of every hypercube [36] and that we are considering two colours. When the system is completely saturated with fermions, any further increase of the chemical potential will be totally ineffective: the fermions are completely frozen and the gluons are the only dynamical degrees of freedom. Then the observables take on their quenched values at $\mu > \mu_s$ and, in particular, the topological susceptibility grows again until reaching a second plateau. In fact the corresponding temperature for the quenched theory lies in the confined phase where χ is nonzero [14]. However it is important to notice that the saturation point is an unphysical effect related to the countable number of sites in the lattice or, stated otherwise, to the presence of an ultraviolet (UV) cutoff, and is thus expected to disappear in the continuum limit; an essential point is that in our case the saturation point μ_s turns out to be larger than the critical chemical potential μ_c and also well separated from it, so that the study of the deconfinement phase transition is not affected by that lattice artifact.

The paper is organized as follows: in Section 2 the technical details of the numerical simulations are given; the calculation of χ and the investigation of its behaviour across the transition are presented in Section 3 together with the extraction of the physical units. Section 3 also contains a study of simultaneity of the chiral, confinement and topological transitions. Some conclusive comments are left for the last Section.

II. MONTE CARLO SIMULATIONS

We have performed numerical simulations in QCD with dynamical staggered quarks [35]. Following Ref. [23] we have worked with two colours and 8 flavours of staggered fermions. The action is [37]

$$S = \frac{1}{2}\sum_x \eta_4(x)\Big\{\mathrm{e}^{a\mu}\overline{\psi}(x)U_4(x)\psi(x+\widehat{4}) - \mathrm{e}^{-a\mu}\overline{\psi}(x+\widehat{4})U_4(x)^\dagger\psi(x)\Big\}$$

$$+\frac{1}{2}\sum_{i=1}^{3}\sum_x \eta_i(x)\Big\{\overline{\psi}(x)U_i(x)\psi(x+\widehat{i}\,) - \overline{\psi}(x+\widehat{i}\,)U_i(x)^\dagger\psi(x)\Big\}$$

$$+am\sum_x \overline{\psi}(x)\psi(x) + S_W\,, \tag{2.1}$$

where $\eta_\nu(x)$ are the staggered phases and $U_\nu(x)$ are the gauge links starting at site x and directed towards $\widehat{\nu}$. S_W is the usual Wilson action for gauge fields [38]. Fermion fields have been multiplied by a suitable power of the lattice spacing a in order to render them dimensionless.

For further details on the algorithm and the action we refer the reader to Ref. [23]. We remind the reader that the chiral symmetries of the lattice action are not equal to the ones of the corresponding continuum theory.

We have numerically simulated the model on a $14^3 \times 6$ lattice at inverse bare gauge coupling $\beta \equiv 4/g^2 = 1.5$ and bare quark mass $am = 0.07$ by using the Hybrid Molecular Dynamics (HMD) algorithm [39]. The presence of a chemical potential prevents us from separating odd and even sites [40] and as a consequence we worked with 8 flavours. We have not used the square root trick to reduce the number of quark species.

We have run the Molecular Dynamics algorithm with step size $\delta\tau = 0.02$ [23] and 50 decorrelation HMD steps have been performed between two successive measurements. This separation was chosen so to have configurations with well–decorrelated topological properties [41–43]. For a few values of μ, 100 HMD steps were used.

Although we have used a non–exact algorithm, possible systematic errors due to the finite step size seem to be under control. This statement is corroborated by two facts: *i)* runs corresponding to the same input parameters but with finer HMD step size ($\delta\tau = 0.005$) have been carried out and results remain stable; *ii)* at large chemical potential, where the theory becomes effectively quenched, our results are in complete agreement with similar measurements obtained from separate runs performed by simulating the pure gauge action, (see Section 3.c).

We have calculated the topological susceptibility from the fluctuations of the topological charge, estimated by using the 1–smeared operator (see next Section). We also measured the

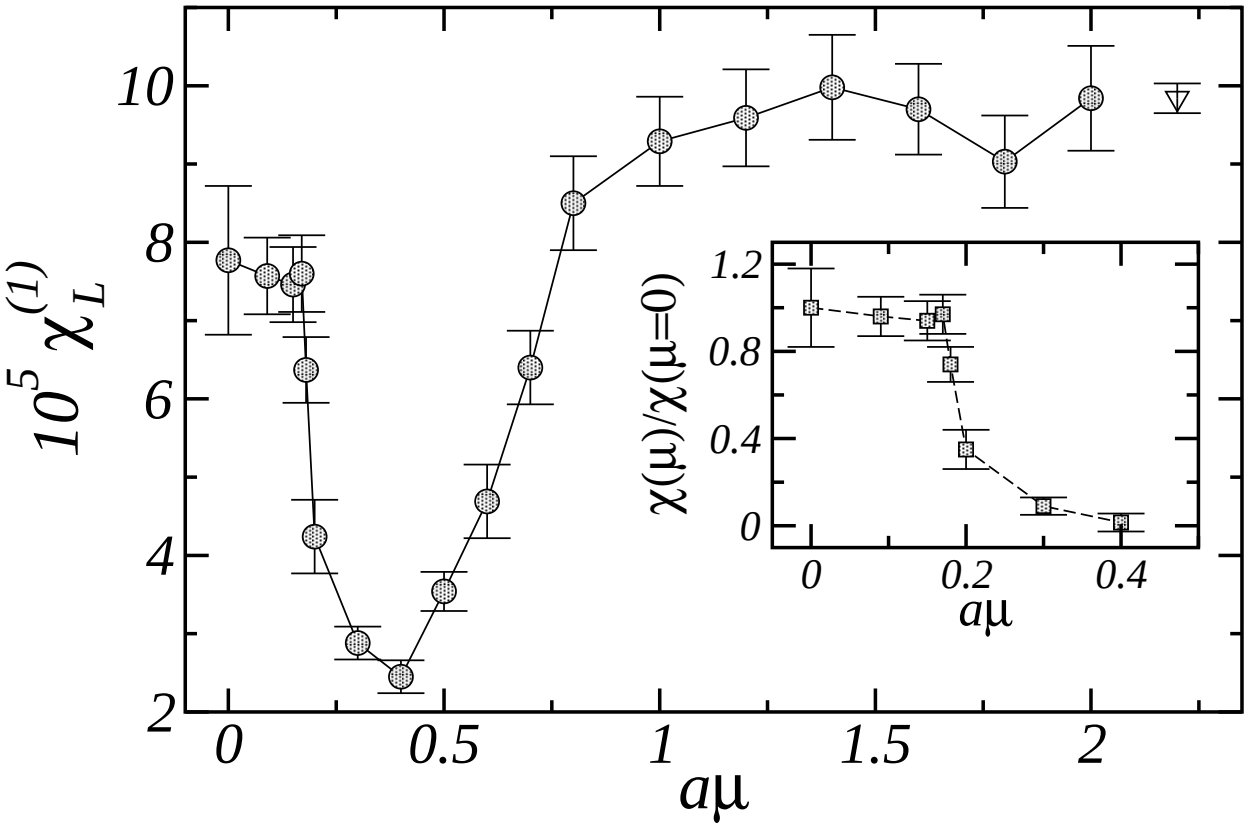

FIG. 1. $\chi_L^{(1)}$ (circles) as a function of the adimensional chemical potential $a\mu$. The last point (empty down triangle) is the value of $\chi_L^{(1)}\big|_{\rm quenched}$ at the same β. In the inset the ratio $\chi(\mu)/\chi(\mu=0)$ (squares) is shown in the interval of $a\mu$ where no apparent effects of Pauli blocking are detectable. Lines are drawn to guide the eye.

Polyakov loop, the average plaquette, the baryon density and the chiral condensate. Depending on the value of $a\mu$, the statistics for these observables was 300–500 uncorrelated measurements.

Early exploratory runs indicate that on a $14^3 \times 6$ lattice at $\beta = 1.5$, $am = 0.07$ and zero chemical potential, the system is in the normal hadronic phase. According to the suggested phase diagram for two colour QCD in the temperature–density plane (Fig. 1 of Ref. [44]), our simulations will cross a transition line which separates the hadronic phase from another state. Depending on the temperature, this state can be either the quark–gluon plasma or the superfluid state and the respective transition can change its nature correspondingly. In

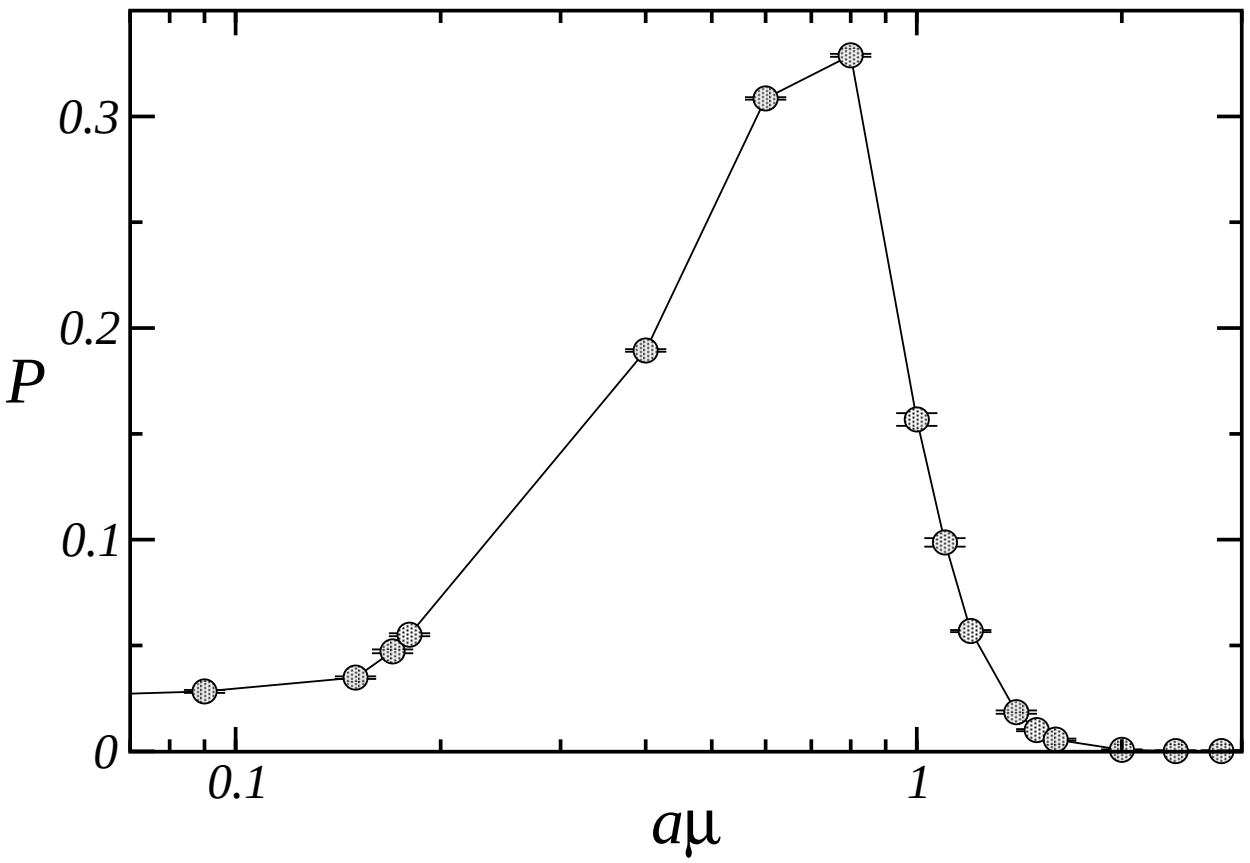

FIG. 2. Polyakov loop P as a function of $a\mu$. The logarithmic scale allows to disentangle the data obtained in the vicinity of the transition point. Points are joined by a line to guide the eye.

the present work we have not examined the order of this transition but we have shown that the transitions for the Polyakov loop, chiral condensate and topological susceptibility are concomitant. From this fact and the calculated value of the ratio T/T_c (see later) we infer that possibly our system becomes a deconfined plasma of quarks and gluons for $\mu > \mu_c$ (T_c is defined as the temperature where the chiral vector symmetry is restored at zero chemical potential). Moreover the fermionic saturation is consistently observed at roughly the same value μ_s for all observables.

III. MEASUREMENT OF χ AND ITS BEHAVIOUR ACROSS THE TRANSITION

A. The method

The first task to calculate the topological susceptibility on the lattice is the introduction of a regularized topological charge density operator $Q_L(x)$. We require that this operator satisfies the continuum limit (in the operator sense) $Q_L(x) \stackrel{a\to 0}{\longrightarrow} a^4 Q(x)$ where a is the lattice spacing. By calling $Q_L \equiv \sum_x Q_L(x)$ the lattice topological susceptibility is defined as

$$\chi_L \equiv \frac{\left\langle \, (Q_L)^2 \, \right\rangle}{V} \,, \tag{3.1}$$

where V is the spacetime volume of the lattice. This quantity is not yet equal to the physical susceptibility χ. They are related through the general expression [45]

$$\chi_L = Z^2 \, a^4 \, \chi + M \,, \tag{3.2}$$

where Z and M are renormalization constants usually called multiplicative and additive respectively. They depend on the lagrangian (specifically on the quark masses and the gauge coupling) and on the operator used on the lattice to regularize the topological charge. In particular had we used an operator $Q_L(x)$ suggested by a fermion theory obeying the Ginsparg–Wilson condition [46,47] then Z would have become equal to 1 and M equal to zero [48]. We did not make use of such operators because their calculation on the lattice is very demanding in computer time.

In order to obtain χ from Eq. (3.2) we have used the Pisa method (also called "field–theoretical method"). In this method one first calculates Z and M and then inserts their values in Eq. (3.2), to extract the result for $a^4\chi$.

Let us explain the origin of Z and M in Eq. (3.2). Let $G^{(n,l)}(p_1, p_2, \cdots; q_1, q_2 \cdots)$ be a bare Green's function with n elementary fields (carrying momenta p_i) and l insertions of the topological charge density operator (carrying momenta q_i) to be computed in the quenched theory. This function can be calculated either in the continuum by using some regularization

method or on the lattice. In both cases the inclusion of renormalization constants for the external fields and gauge coupling is enough to make the Green's function finite (because the calculation is performed in the quenched theory where $Q(x)$ is a renormalization group invariant operator). Let us call $G^{(n,l)}_{R,\mathrm{lattice}}$ and $G^{(n,l)}_{R,\mathrm{continuum}}$ the two renormalized functions thus obtained. In general, for an arbitrary renormalization scheme, the two functions $G^{(n,l)}_{R,\mathrm{lattice}}$ and $G^{(n,l)}_{R,\mathrm{continuum}}$ are not necessarily equal and they match only after the inclusion of a multiplicative finite renormalization constant Z [49,50] for each of the l insertions of topological charge operator. In a formal writing: $Q_L(x) = Za^4Q(x)$. When $l > 1$ there may be further divergences originated by contact terms, see later.

In the theory with fermions the topological charge mixes with other operators related to the axial anomaly [51]. This mixing induces a correction to the above described multiplicative renormalization. Such a correction is however rather small [52] and we neglect it, consistently with the large statistical and systematic errors of our numerical simulation.

The r.h.s. of Eq. (3.1) contains the product of two operators at the same spacetime point. In Field Theory such products can be divergent [53]. On the other hand the correlator $\langle Q(x)Q(0)\rangle$ is negative for $x \neq 0$ as shown in [54–56]. Also on the lattice this correlator is negative [57–59]. Then part of the contact divergences must add up to the total topological susceptibility in order to make it positive. The rest of the contact divergences, if any, must be subtracted. This subtraction is M. In order to calculate it, we can follow the strategy introduced in [61,14]: M is the value of χ_L in the sector of zero total topological charge, $M \equiv \chi_L\Big|_{Q=0}$. This prescription guarantees the physical requirement that χ vanishes in such a sector. M can be also calculated in nonzero topological charge sectors [62] yielding concordant results. Although M consists of UV divergences, it turns out to be a finite quantity because we are working on the regularized theory (in the practical calculation the cutoff a is never sent to zero).

We have calculated the topological susceptibility for several values of the chemical potential at a fixed inverse gauge coupling β. This entails that the additive and multiplicative renormalization constants must be the same for all values of μ. Since we will present the res-

Table 1

Measurements of several operators for varying μ.

$a\mu$	$10^5\,\chi_L^{(1)}$	$10^5\,M$	$a^3\rho_B$	$\langle\frac{1}{2}\mathrm{Tr}\Box\rangle$	$\langle\overline{\psi}\psi\rangle_{\mathrm{full}}$	$\langle\overline{\psi}\psi\rangle_{\mathrm{quenched}}$	P
0.0	7.77(95)	2.54(19)	0.001(1)	0.4621(2)	0.592(2)	0.904(3)	0.023(1)
0.09	7.57(49)	–	–	0.4627(3)	0.587(2)	–	0.0283(7)
0.15	7.46(48)	–	–	0.4631(2)	0.581(2)	–	0.0348(6)
0.17	7.60(49)	–	0.005(1)	0.4647(4)	0.568(2)	–	0.0472(9)
0.18	6.37(42)	–	0.006(2)	0.4665(2)	0.552(2)	–	0.0551(7)
0.2	4.24(47)	2.29(19)	–	–	–	–	–
0.3	2.88(21)	–	–	–	–	–	–
0.4	2.45(21)	2.16(13)	0.060(2)	0.4912(2)	0.280(1)	0.493(3)	0.1894(6)
0.5	3.54(25)	–	–	–	–	–	–
0.6	4.69(47)	2.73(19)	0.230(2)	0.4764(2)	0.105(1)	–	0.3085(6)
0.7	6.40(47)	–	–	–	–	–	–
0.8	8.50(60)	–	0.554(2)	0.415(2)	0.062(1)	0.059(9)	0.3289(7)
1.0	9.29(57)	–	0.882(2)	0.3742(5)	0.015(3)	0.005(1)	0.157(3)
1.1	–	–	0.958(1)	0.3668(3)	0.003(1)	0.003(1)	0.099(2)
1.2	9.59(62)	–	0.987(1)	0.3638(1)	0.0014(3)	$3(5)\,10^{-4}$	0.057(1)
1.4	9.98(67)	–	0.998(1)	0.3626(4)	0.0012(4)	$3(3)\,10^{-4}$	0.019(1)
1.5	–	–	0.999(1)	0.3626(1)	$1(2)\,10^{-4}$	–	0.010(1)
1.6	9.70(58)	–	1.000(1)	0.3625(1)	$-2(2)\,10^{-4}$	$-3(2)\,10^{-4}$	0.006(1)
1.8	9.03(59)	–	–	–	–	–	–
2.0	9.83(67)	–	1.000(1)	0.3625(1)	$3(5)\,10^{-5}$	–	$7(2)\,10^{-4}$
2.4	–	–	0.999(1)	0.3624(1)	$6(6)\,10^{-5}$	–	$1(4)\,10^{-4}$
2.8	–	–	1.000(1)	0.3623(1)	$3(4)\,10^{-5}$	–	$1(4)\,10^{-4}$
3.2	–	–	1.000(1)	0.3626(1)	$2(3)\,10^{-5}$	$-1(1)\,10^{-4}$	$3(4)\,10^{-4}$

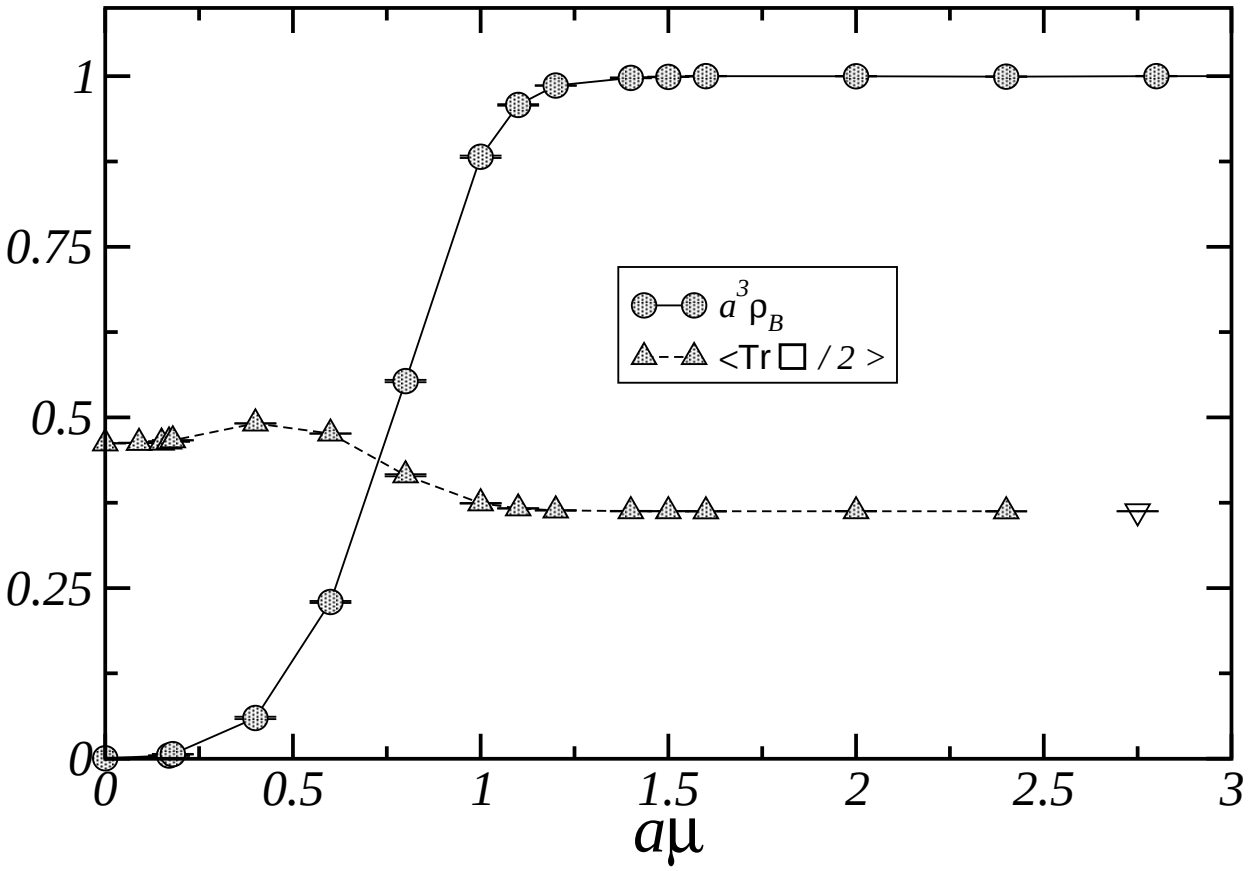

FIG. 3. Baryonic density $a^3\rho_B$ (circles) and plaquette $\langle\frac{1}{2}\mathrm{Tr}\Box\rangle$ (up triangles) as a function of $a\mu$. The last point (empty down triangle) is the value of the plaquette for the quenched theory at the same β value. Lines are drawn to guide the eye.

ults for the ratio $\chi(\mu)/\chi(\mu = 0)$ as a function of μ, the multiplicative Z needed not be calculated (the notation $\chi(\mu)$ indicates the physical topological susceptibility at a value μ of the chemical potential). Instead M was calculated by use of the heating method [60,61]. This method consists in the following: we started with the trivial configuration (all links equal to unity) which clearly belongs to the zero topological sector. Then we applied 5000 steps of HMD updating and measured χ_L every 100 steps. This set of 50 measurements is called "trajectory". After each measurement we applied also 8 cooling steps [45,63,64] and determined Q_L and the total energy of the configuration to verify that the topological sector was not changed (other methods to check the background topological sector, like the counting of fermionic zero modes [65], yield the same results for M and Z). We repeated the whole

procedure to obtain a number of trajectories. For each trajectory we always discarded the first few measurements because the configuration was not yet thermalized[†]. Averaging over the thermalized steps (as long as the corresponding cooled configuration showed the correct topological charge sector, $Q = 0$ within a deviation δ) yielded $\chi_L\Big|_{Q=0}$. We estimated the systematic error that stemmed from the choice of δ as in Ref. [14].

When the cooling (or other) test reveals that a configuration has moved from the zero topological charge sector to another sector, it is discarded. Actually this event seldom happens because the topological modes are effectively decoupled from the UV modes so that after starting from a classical configuration of any fixed topological content, it is difficult to alter the background topological sector by applying some updating (heating) steps at the corresponding value of β to thermalize the UV fluctuations. In fact this decoupling of the two types of modes is the gist of the heating method [60,61].

B. The lattice operator

A valid lattice regularization of the topological charge density operator, Eq. (1.1), is given by [66]

$$Q_L(x) = -\frac{1}{2^9\pi^2}\sum_{\zeta\nu\gamma\sigma=\pm1}^{\pm4}\widetilde{\epsilon}_{\zeta\nu\gamma\sigma}\mathrm{Tr}\left\{\Pi_{\zeta\nu}(x)\Pi_{\gamma\sigma}(x)\right\}\ , \tag{3.3}$$

where $\Pi_{\zeta\nu}(x)$ is the plaquette in the $\zeta-\nu$ plane with the four corners at x, $x+\widehat{\zeta}$, $x+\widehat{\zeta}+\widehat{\nu}$, $x+\widehat{\nu}$ (counter–clockwise path). As indicated in the sum, indices ζ, ν, γ and σ can point towards either positive or negative directions. Links pointing to negative directions mean $U_{-\nu}(x) \equiv U_\nu^\dagger(x-\widehat{\nu})$. The generalized completely antisymmetric tensor is defined by $\widetilde{\epsilon}_{1234} = 1$ and $\widetilde{\epsilon}_{(-\zeta)\nu\gamma\sigma} = -\widetilde{\epsilon}_{\zeta\nu\gamma\sigma}$.

[†]In this context thermalization is defined with respect to short range fluctuations within the zero topological charge sector.

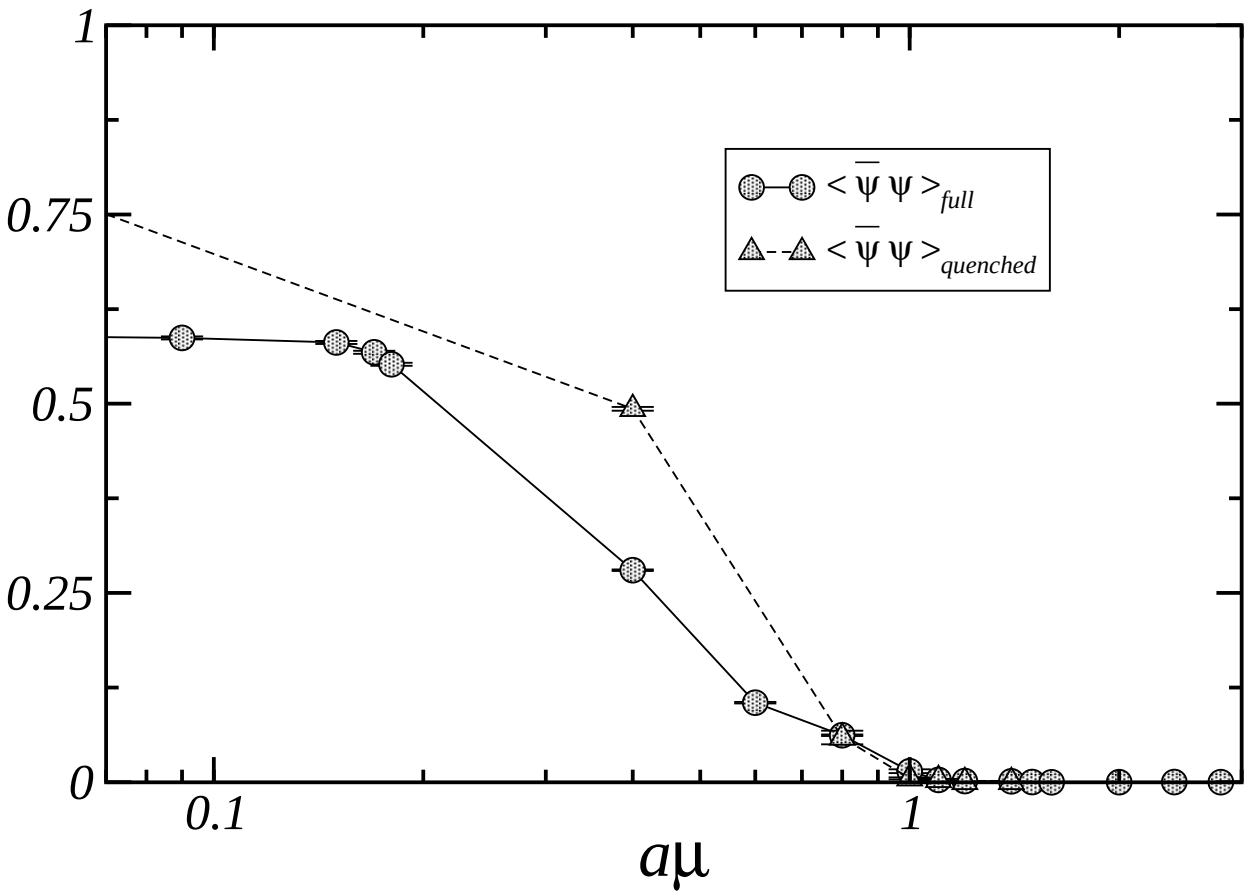

FIG. 4. Chiral condensate for the full theory (circles) and the quenched theory (triangles) as a function of $a\mu$. The logarithmic scale allows to disentangle the data obtained in the vicinity of the transition point. Lines are drawn to guide the eye.

The lattice operator used in our simulations was the 1–smeared $Q_L^{(1)}(x)$ which is constructed from Eq. (3.3) after substituting all link matrices by 1–smeared links [67]. If $U_\nu(x)$ is the link starting at site x and pointing towards the $\widehat{\nu}$ direction, the 1–smeared link $U_\nu^{(1)}(x)$ is defined by the following linear combination of the seven shortest paths connecting the points x and $x+\widehat{\nu}$

$$\overline{U}_\nu(x) \equiv (1-c)U_\nu(x) + \frac{c}{6}\sum_{\substack{\alpha=\pm 1 \\ |\alpha|\neq\nu}}^{\pm 4} U_\alpha(x)U_\nu(x+\widehat{\alpha})U_\alpha^\dagger(x+\widehat{\nu})\,,$$

$$U_\nu^{(1)}(x) \equiv \frac{\overline{U}_\nu(x)}{\left(\frac{1}{2}\mathrm{Tr}\overline{U}_\nu^\dagger(x)\overline{U}_\nu(x)\right)^{1/2}}\,. \tag{3.4}$$

This combination is then projected back onto SU(2) as indicated by the second line in

Eq. (3.4). By using smeared operators less noisy results are obtained. The parameter c can be tuned in order to optimize this improvement. We chose $c = 0.85$ as in [13]. The naïve continuum limit of $Q_L^{(1)}(x)$ equals the continuum topological charge density, Eq. (1.1).

Following the definition (3.1) we called $Q_L^{(1)} \equiv \sum_x Q_L^{(1)}(x)$ the total 1–smeared lattice topological charge and

$$\chi_L^{(1)} \equiv \frac{\left\langle \left(Q_L^{(1)}\right)^2 \right\rangle}{V} \tag{3.5}$$

the 1–smeared lattice topological susceptibility. $\chi_L^{(1)}$ and $a^4\chi$ are related by Eq. (3.2). We have calculated M for four values of μ as shown in Table 1. Averaging over all four results leads to $M(\beta = 1.5, am = 0.07) = 2.37(8) \times 10^{-5}$. This is the value of M that we have used throughout the paper.

C. The Monte Carlo simulation

In Fig. 1 the results for $\chi_L^{(1)}$ are shown as a function of $a\mu$. Data are given in Table 1. The sudden drop at $a\mu_c = 0.175(5)$ is apparent. In the inset of Fig. 1 we show the scaling ratio $\chi(\mu)/\chi(\mu = 0)$ for $a\mu \leq 0.4$. Accordingly with Eq. (3.2) this ratio is calculated as

$$\frac{\chi(\mu)}{\chi(\mu = 0)} = \frac{\chi_L^{(1)}(\mu) - M}{\chi_L^{(1)}(\mu = 0) - M}\,. \tag{3.6}$$

The notation $\chi_L^{(1)}(\mu)$ stands for the lattice topological susceptibility, Eq. (3.5), calculated at chemical potential μ. This inset is one of the two main results of our paper: it displays the drop of the physical topological susceptibility. Notice that the results in this plot are free from Z and a^4 factors.

In Fig. 2 the Polyakov loop is shown in a similar range of values of chemical potentials at the same β and quark mass. All data are listed in Table 1. The rise of the Polyakov loop displayed by this Figure happens at a value of $a\mu$ which is compatible within errors with the value of $a\mu_c$ at which $\chi(\mu)$ drops.

For values of the chemical potential larger than $a\mu = 0.5$, the topological susceptibility begins to increase again and then flattens at $a\mu \gtrsim 1.2$, as shown in Fig. 1. Such a value

corresponds to the saturation point, μ_s. This new plateau is not the indication of a new physical phase. It is due to the Pauli blocking, a saturation of the fermion number throughout the lattice. The value for the chemical potential is so high that the baryon density ρ_B reaches the maximum allowed value, 1 baryon per site. After this point the fermions are frozen and the theory is entirely analogous to the quenched theory. To say it plainly, simulating the theory at those high values of μ is nothing but a clumsy way to reproduce the SU(2) pure gauge theory.

The above qualitative argument is validated by Monte Carlo simulations of the pure gauge theory that compare very well with the full theory simulated at $\mu \gtrsim \mu_s$. In particular the empty down triangle in Fig. 1 is the value of $\chi_L^{(1)}$ calculated in a separate simulation by using the SU(2) pure gauge Wilson action, its value being $\chi_L^{(1)}\Big|_{\rm quenched} = 9.84(19)\,10^{-5}$. The agreement between this number and the last data for $a\mu \gtrsim 1.2$ is manifest. Also the signal for the Polyakov loop in Fig. 2 disappears at $a\mu \gtrsim 1.2$. This is the expected behaviour for this operator in the quenched theory when, as in our case, the temperature is below deconfinement, $T < T_c$.

The rise of the signal of $\chi_L^{(1)}$ for $\mu \lesssim \mu_s$ is slow in contrast with its sudden drop at μ_c. This effect is due to the partial blocking of fermions which increases with μ until it reaches the total saturation at μ_s.

Notice that the saturation of the fermion degrees of freedom makes the theory to behave as the pure gauge theory in all respects. In particular not only $\chi_L^{(1)}$ assumes the quenched value, but also the renormalization constants and the beta function do (i.e.: the full theory becomes quenched, also perturbatively), in such a way that the physical susceptibility χ turns into that of the pure gauge theory too.

The saturation of fermions and subsequent forced quenching of the theory is due to the fact that on the lattice there are a finite number of physically accessible sites. Hence it is an unphysical lattice effect with no counterpart in the continuum. It is interesting to notice that the effective quenching at large values of $\mu > \mu_s$ corresponds to the fermionic determinant becoming a constant independent of the gauge field background; this can be

easily understood looking at the fermionic part in Eq. (2.1): in the large μ limit the forward temporal part of the Dirac matrix is exponentially larger than the other terms, and the determinant of a matrix containing only the forward temporal part is indeed independent of the gauge field background, as can be easily verified.

In Fig. 3 we show the data for the baryonic density $a^3\rho_B$ and the plaquette $\langle \frac{1}{2}\mathrm{Tr}\Box \rangle$ versus the chemical potential. Both data sets can be found in Table 1. At the saturation point, $a\mu_s \approx 1.2$, the density attains the maximum value $a^3\rho_B = 1$ and the plaquette becomes that of the quenched theory. This value of $a\mu_s$ is roughly the same at which the topological susceptibility begins the second plateau in Fig. 1 and the Polyakov loop becomes zero in Fig. 2. The quenched value of the plaquette at $\beta = 1.5$ has been calculated in a separate simulation with the pure gauge Wilson action and it is shown as an empty triangle in Fig. 3. It amounts to $\langle \frac{1}{2}\mathrm{Tr}\Box \rangle_{\mathrm{quenched}} = 0.362432(23)$ which is in perfect agreement with the (Pauli blocked) values of the average plaquette in the full theory for $\mu > \mu_s$, (see Table 1).

All observables agree with their corresponding quenched values as soon as the chemical potential is high enough to induce fermionic saturation. We have also calculated the chiral condensate as a function of $a\mu$. The results are shown in Table 1 and Fig. 4 for both the full and quenched theories. In the two simulations, we have measured the same operator, i.e. the trace of the inverse of the (μ–dependent) quark matrix. In one case it was calculated by using configurations obtained from the full theory and in the other case by using configurations corresponding to the pure gauge theory. In the full theory the condensate drops at the same $a\mu_c$ where the Polyakov loop rises and the topological susceptibility falls abruptly. Thus the three operators undergo their transitions at the same density. We are aware that neither the Polyakov loop nor the topological susceptibility are order parameters for confinement and the singlet flavour $\mathrm{U_A}(1)$ symmetry respectively. In particular the drop of the signal of the topological susceptibility does not necessarily mean a restoration of the $\mathrm{U_A}(1)$ symmetry although it must have physically measurable consequences in observables directly related to χ. This set of consequences is commonly termed as "effective restoration" of the $\mathrm{U_A}(1)$ symmetry [9,11].

For values of the chemical potential larger than the saturation point μ_s the chiral condensate in the full theory stays vanishingly small. This behaviour coincides with that of the chiral condensate calculated in the quenched theory as shown in Fig. 4. Notice that in the present case, the operator depends on the chemical potential and this is why we show the data for the quenched model as a function of $a\mu$. However as soon as the chemical potential reaches the saturation value the two sets of data become coincident. This is another indication that the full theory at $\mu > \mu_s$ becomes entirely quenched. In the quenched case a straightforward algebra yields the leading dependence for large μ

$$\langle\overline{\psi}\psi\rangle_{\rm quenched} \propto {\rm e}^{-N_t a\mu}\,, \tag{3.7}$$

where N_t is the lattice temporal extent, $N_t = 6$ in our case.

D. The numerical results

We have also given approximate physical units to the lattice spacing a and therefore also to the critical value of the chemical potential μ_c. In a separate Monte Carlo simulation we have calculated the chiral condensate and the Polyakov loop as a function of the temperature at zero chemical potential. To this end we have kept fixed the temporal lattice size and have varied the gauge coupling β. In Fig. 5 and Table 2 we show the results of the simulation. From the position of the flex point in any of the two curves of this Figure we can extract the critical beta, $\beta_c = 1.594(6)$. By taking into account the two loop beta function of the model (Λ_L is the renormalization group invariant mass scale corresponding to the bare lattice coupling of the action (2.1)),

$$a(\beta)\Lambda_L = {\rm e}^{-\pi^2\beta}\left(\frac{1}{2\pi^2\beta}\right)^{5/2}\left[1 + O\left(\frac{1}{\beta}\right)\right]\,, \tag{3.8}$$

we obtain the ratio $a(\beta_c)/a(\beta = 1.5) = 0.34(3)$ where the error comes from the imprecision in the determination of β_c (notice that we use indistinctly the notation a or $a(\beta)$). The error caused by the ignorance of higher loop terms in the beta function is rather small within the

narrow interval between $\beta = 1.5$ and β_c (actually the sole one loop term is enough to account for about the 85% of the variability of the function $a(\beta)$ in that interval).

Since our simulations have been performed at $\beta = 1.5$ on a lattice of time size equal to 6, the temperature of our system was $T/T_c = a(\beta_c)/a(\beta = 1.5) = 0.34(3)$ and the resulting value for the critical chemical potential was $\mu_c/T_c = 6 \times (T/T_c) \times 0.175(5) = 0.357(10)(32)$ where the first error is due to the Monte Carlo determination of the critical value of $a\mu$ and the second one derives from the error in β_c.

From Table 1 we can also give an approximation for the critical density. Since the transition lies between $a\mu = 0.17$ and $a\mu = 0.18$, from Table 1 we can approximate the density at the transition point as $a^3\rho_{B,c} = 0.0055(15)$ which is the average of $a^3\rho_B$ among the two values of $a\mu$. From this average we obtain $\rho_{B,c}/T_c^3 = 6^3 \times (T/T_c)^3 \times 0.0055(15) = 0.047(13)(12)$ where the first error comes from the lattice determination of $a^3\rho_{B,c}$ and the second one is due to the determination of β_c.

Based on the large number of fermions in our lagrangian and on the fact that they are quite heavy, we surmise that the critical temperature for our system at zero chemical potential is $T_c = 100-200$ MeV. Then the value of the lattice spacing at β_c is $a(\beta_c) = 1/6T_c = 0.00111(^{+56}_{-28})$ MeV^{-1}. From the ratio T/T_c we obtain the value of the lattice spacing in our simulation runs, $a(\beta = 1.5) = 0.00327(22)(^{+165}_{-83})$ MeV^{-1} $= 0.64(4)(^{+33}_{-16})$ fm where the first error is due to the imprecision on β_c and the second one to the estimated inaccuracy on T_c.

We see that our lattice is coarse. It is a consequence of the small lattice size (due to computer limitations) and of the need to work at $T < T_c$ in order to run into a phase transition while μ is increasing.

Notice that within the above limits for T_c, the value of the critical fermion chemical potential μ_c ranges from 36(1)(3) to 72(2)(6) MeV. Then the critical baryonic chemical potential $\mu_{B,c} = 2\mu_c$ varies from 70 to 145 MeV at a temperature $T/T_c = 0.34(3)$, indicating a curvature of the phase boundary in the μ–T plane quite larger than what is measured in QCD with three colours: that does not come as a surprise, since in two colour QCD baryon states are degenerate with mesons [68], so that the critical chemical potential at zero

temperature may well be lower than in usual QCD.

Table 2

Measurements of $\langle\overline{\psi}\psi\rangle_{\rm full}$ and P for varying β at $\mu = 0$.

β	$\langle\overline{\psi}\psi\rangle_{\rm full}$	P
1.525	0.5521(19)	0.030(1)
1.55	0.5080(25)	0.038(1)
1.5625	0.4828(25)	0.0402(35)
1.575	0.4466(26)	0.0549(23)
1.5875	0.4131(30)	0.0685(10)
1.6	0.3735(22)	0.0880(18)
1.6125	0.3454(24)	0.1041(20)
1.625	0.3279(15)	0.1082(20)
1.65	0.3005(8)	0.1208(10)
1.675	0.2801(7)	0.1315(7)

By allowing the valuation of T_c to vary in such a wide range (100–200 MeV) we have mimicked an estimate of the systematic error derived from the great number of quark species and their big mass. There are however other sources of systematic errors which have not been contemplated in the present analysis: the (wrong) gauge group, the large value of the lattice spacing, the modest size of the lattice volume and the use of a non–exact updating algorithm. The experience in simulating and comparing the physics of SU(2) and SU(3) gauge theories teaches us that the first problem is possibly unimportant with regard to the behaviour of the topological susceptibility. As described above, the main influence of the wrong gauge group regards the numerical values of the physical parameters. The second and

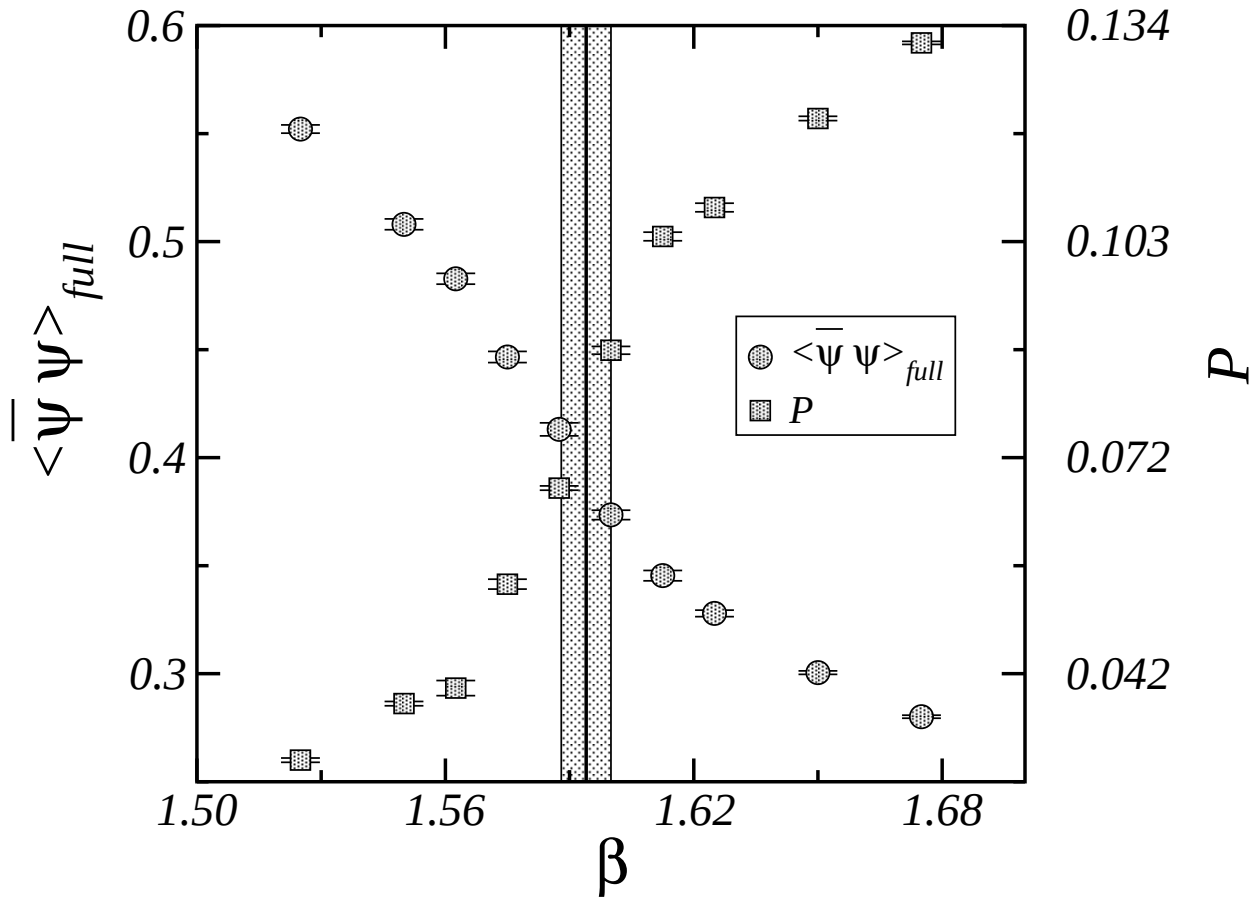

FIG. 5. Chiral condensate (circles and left vertical axis) and Polyakov loop (squares and right vertical axis) as a function of β at vanishing chemical potential in the neighbourhood of the finite temperature transition. The vertical line and band are the value of β_c and its error.

third problems can be ameliorated by studying the theory on larger volumes. We think that none of these errors can change the two main conclusions of our paper: the drop of the topological susceptibility at the transition and the coincidence of all transitions.

E. Relationship between transitions

We have claimed that the three transitions studied in the present paper, namely the one related to topology, to the Polyakov loop and to the chiral condensate are concomitant: they all happen at about the same value of the chemical potential. We substantiate this statement with the help of the plot shown in Fig. 6. In this plot we display the derivatives

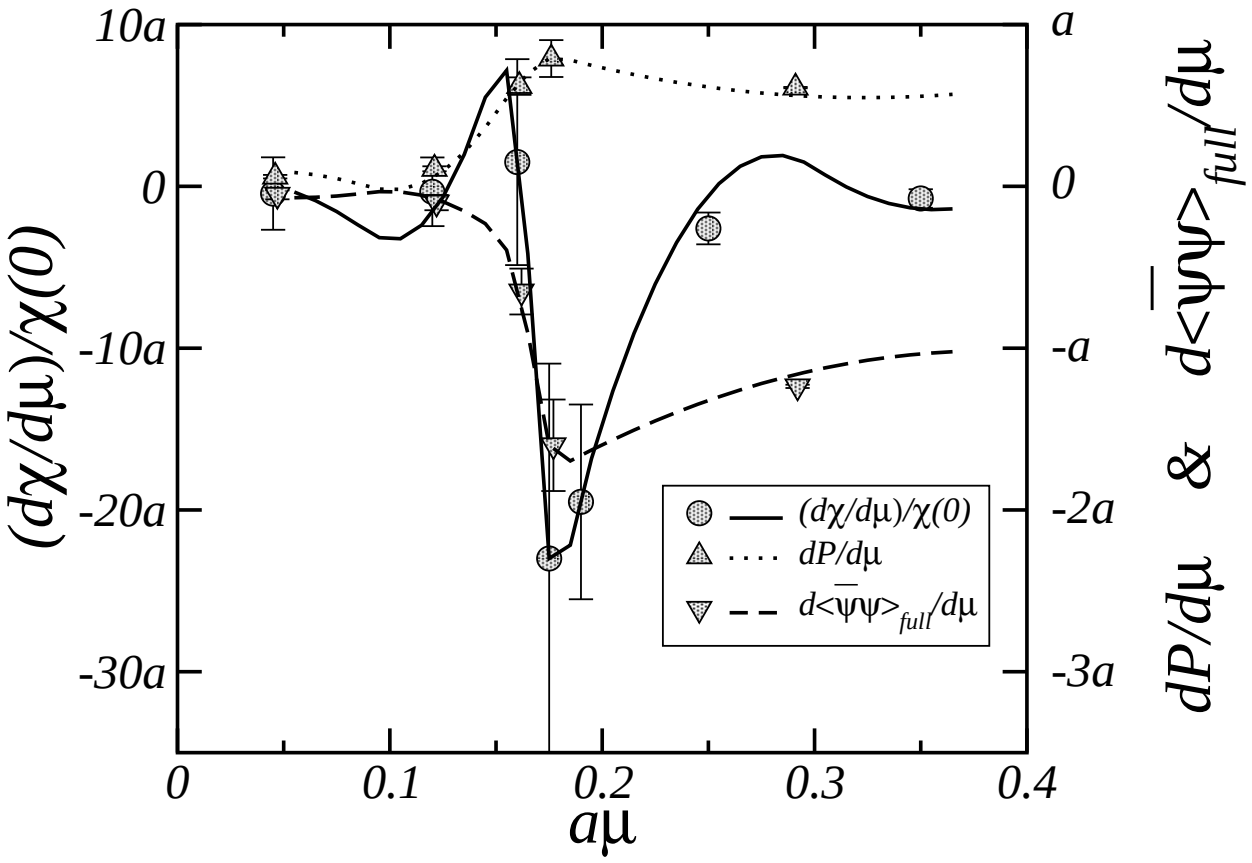

FIG. 6. Derivatives with respect to the chemical potential μ of the normalized topological susceptibility (circles, continuous line and left vertical axis), Polyakov loop (up triangles, dotted line and right vertical axis) and chiral condensate (down triangles, dashed line and right vertical axis). The two vertical axes are expressed in units of the lattice spacing a. The three sets of data have been slightly shifted horizontally to avoid the overlapping of various symbols and error bars. Lines are the result of the interpolation described in the text.

of the three observables (with immaterial proportionality constants) with respect to the chemical potential. If the transitions are identified as the points where the variations are sharper then the Figure seems to give unquestionably evidence in favour of the coincidence for the three transitions. This conclusion is the second main result of the paper.

The plot is shown within the interval of chemical potentials spanning from 0 to the maximum μ where no Pauli blocking effects are apparent. The isolated points (circles, up and down triangles) for the observable O ($\chi(\mu)/\chi(0)$, P or $\langle\overline{\psi}\psi\rangle_{\rm full}$) have been obtained by

calculating the discrete derivative

$$\frac{O(\mu_i) - O(\mu_{i-1})}{\mu_i - \mu_{i-1}} \tag{3.9}$$

from the data in Table 1 and placing the result at position $a(\mu_i + \mu_{i-1})/2$. Furthermore Monte Carlo data for each observable have been interpolated by a natural cubic spline [69]. Then the derivative of these interpolation functions have been calculated and they are the lines plotted in Fig. 6. All three lines and all three sets of data points show a clear peak at the same value $a\mu_c = 0.175$. The continuous line, which corresponds to the topological susceptibility, displays other points with a large derivative. This is an spurious effect on the spline interpolation due to the fluctuation that makes the value of χ_L at $a\mu = 0.17$ to move upward a little bit, see Fig. 1.

A similar figure can be drawn for pure gauge theories and for full QCD indicating that the concomitancy is a common feature of the three kinds of transition for all theories that we have studied up to date [70].

IV. CONCLUSIONS AND OUTLOOK

We have studied on the lattice the behaviour of the topological susceptibility χ in QCD with two colours and 8 flavours of quarks as a function of the quark chemical potential μ at finite temperature. The so–called sign problem hinders a similar investigation in full QCD with three colours.

Previous studies of topology in Yang–Mills theories at finite temperature for two and three colours both with or without fermions have shown that χ undergoes an abrupt drop at the deconfinement phase transition. The results of our paper indicate that a similar quick drop takes place also at the finite density phase transition, (see inset in Fig. 1). It happens at a value of the chemical potential $a\mu_c = 0.175(5)$. This value of μ is the same at which the Polyakov loop and the chiral condensate undergo sudden changes (see Fig. 2 and Fig. 4). The rise of the Polyakov loop demonstrates enhanced screening possibly compatible with

deconfinement and the chiral condensate exhibits a behaviour that is compatible with a restoration of flavour chiral symmetry (see Fig. 4).

If the chemical potential is further increased, the topological susceptibility rises again as more and more fermions are inserted into the system. We have given compelling arguments showing that this rise is not the signal of a new physical phase but just an artifact of the UV regularization of the lattice, which makes the number of accessible fermion levels finite. Indeed at the saturation point μ_s (for our choice of parameters $a\mu_s \approx 1.2$) the system is completely packed with fermions whose dynamics, due to the Pauli principle, gets frozen. Therefore for $\mu > \mu_s$ the gluons are the only dynamical degrees of freedom and the system behaves as the pure gauge theory at the same value of the gauge coupling and consequently the topological susceptibility takes the corresponding quenched value. In order to support these assertions, we have calculated the baryonic density and verified that it becomes equal to 1 baryon per site for all $\mu > \mu_s$, (see Fig. 3). Similarly, also other observables like the Polyakov loop (Fig. 2), the average plaquette (Fig. 3) and the chiral condensate (Fig. 4) take their quenched values for $\mu > \mu_s$.

We stress that we defined μ_s as the value of the quark chemical potential where saturation becomes complete or, stated otherwise, where the theory becomes quenched.

Since the Pauli saturation of fermions is a pure lattice effect with no counterpart in the continuum, we have not made a detailed study to establish whether its onset corresponds to a true (unphysical) phase transition or not: that may be the subject of further investigation. In fact μ_s must diverge in the continuum limit. Unfortunately this lattice artifact precludes us from making contact with the physics of extremely high densities by numerical simulations.

We have shown that a drop in the signal of the topological susceptibility occurs in the theory with two colours and 8 equal mass flavours. What about the true theory? Due to the similarities in the topology of SU(2) and SU(3) it is conceivable to expect that the drop must be a genuine fact of QCD. Instantons are responsible for the topological properties and they are present in all SU(N) gauge models.

We call T_c the temperature where the chiral vector symmetry is restored at vanishing

chemical potential. By resorting to the above–mentioned similarities between the present model and the true theory of the strong interactions, we have assumed that T_c ranges between 100 and 200 MeV. From this approximation and knowing the value β_c of the gauge coupling at which the chiral symmetry is restored for $\mu = 0$ (see Fig. 5), we have extracted an estimate of the lattice spacing in physical units. Also the ratio $\mu_c/T_c = 0.357(10)(32)$ has been calculated, where the first error is due to the lattice determination of $a\mu$ at the critical point and the second one is derived from the error band in β_c (see Fig. 5). Furthermore $T/T_c = 0.34(3)$. Notice that this ratio is insensitive to the imprecision on T_c. Moreover the baryon density ρ_B at the critical point is $\rho_{B,c}/T_c^3 = 0.047(13)(12)$ where the errors have analogous meanings than those for μ_c/T_c: lattice evaluation of $\rho_{B,c}$ and error on β_c respectively. All the above numerical results are subject to several sources of systematic errors (wrong gauge group, small lattice size, large lattice spacing). Hence we consider them as rough estimates of the true values. However none of the preceding sources of systematic errors is expected to be able to influence the main conclusions of the present paper, namely the drop in the topological susceptibility and the coincidence of this drop with the chiral and Polyakov loop transitions.

By using the assumed limits to the value of the critical temperature at zero chemical potential T_c, the critical baryonic chemical potential $\mu_{B,c} = 2\mu_c$ can be estimated to range from 70 to 145 MeV at $T/T_c = 0.34(3)$. Therefore the value of $\mu_{B,c}$ at zero temperature may be quite lower than what is expected in QCD with three colours. That is not a surprise since in the theory with two colours the lightest baryon state is degenerate with the pion.

We have not studied the order of the transition and the properties of the states at both sides of this transition. On the other hand the number and mass of the quarks in our study are unphysically large. These are important aspects which deserve further analysis because the order of the transition might depend on these parameters.

Our results indicate that the screening of colour forces, chiral symmetry and topology are interrelated in the $T \approx (0.3 - 0.4)T_c$ region of the two colour QCD phase diagram [44]. It would be interesting to repeat this study at other temperatures, in particular at very

small ones where the transition goes from the hadronic to the superfluid phase, which is still confining [71,72], and where chiral symmetry remains broken by a diquark condensate. Such low temperatures, say $T \lesssim 0.1\, T_c$, were not accessible to our simulations because on our lattice sizes it would have required such a large value of the lattice spacing that the results would probably have lost all physical meaning.

V. ACKNOWLEDGEMENTS

It is a pleasure to thank Adriano Di Giacomo for useful comments and discussions. B.A. and M.P.L. also thank Massimo Testa for discussions and B.A. ackowledges Giancarlo Cella for suggestions about the statistical treatment of data. We also thank Michele Pepe for a critical reading of the original draft of the paper and for invaluable help in the simulation runs.

REFERENCES

[1] E. Witten, Nucl. Phys. B156 (1979) 269.

[2] G. Veneziano, Nucl. Phys. B159 (1979) 213.

[3] B. Lucini, M. Teper, U.Wenger, Nucl. Phys. B715 (2005) 461.

[4] L. Del Debbio, L. Giusti, C. Pica, Phys. Rev. Lett. 94 (2005) 032003.

[5] B. Allés, M. D'Elia, A. Di Giacomo, Phys. Rev. D71 (2005) 034503.

[6] S. Narison, hep–ph/0601066.

[7] F. C. Hansen, H. Leutwyler, Nucl. Phys. B350 (1991) 201.

[8] G. M. Shore, G. Veneziano, Nucl. Phys. B381 (1992) 23.

[9] R. D. Pisarski, F. Wilczek, Phys. Rev. D29 (1984) 338.

[10] E. Shuryak, Comments Nucl. Part. Phys. 21 (1994) 235.

[11] M. Marchi, E. Meggiolaro, Nucl. Phys. B665 (2003) 425.

[12] P. Costa, M. C. Ruivo, C. A de Sousa, Yu. L. Kalinovsky, Phys. Rev. D70 (2004) 116013.

[13] B. Allés, M. D'Elia, A. Di Giacomo, Phys. Lett. B412 (1997) 119.

[14] B. Allés, M. D'Elia, A. Di Giacomo, Nucl. Phys. B494 (1997) 281, Erratum: ibid B679 (2004) 397.

[15] B. Allés, M. D'Elia, A. Di Giacomo, Phys. Lett. B483 (2000) 139.

[16] J. Hoek, M. Teper, J. Waterhouse, Phys. Lett. B180 (1986) 112; M. Teper, Phys. Lett. B202 (1988) 553.

[17] L. Del Debbio, H. Panagopoulos, E. Vicari, JHEP 0409 (2004) 028.

[18] A. Di Giacomo, E. Meggiolaro, H. Panagopoulos, Phys. Lett. B277 (1992) 491.

[19] C. Gattringer, R. Hoffmann, S. Schaefer, Phys. Lett. B535 (2002) 358.

[20] Z. Fodor, S. D. Katz, Phys. Lett. B534 (2002) 87; JHEP 0203 (2002) 014.

[21] Ph. de Forcrand, O. Philipsen, Nucl. Phys. B642 (2002) 290; M. D'Elia, M. P. Lombardo, Phys. Rev. D67 (2003) 014505.

[22] C. R. Allton et al., Phys. Rev. D66 (2002) 074507.

[23] S. Hands, J. B. Kogut, M. P. Lombardo, S. E. Morrison, Nucl. Phys. B558 (1999) 327.

[24] J. B. Kogut, D. K. Sinclair, S. J. Hands, S. E. Morrison, Phys. Rev. D64 (2001) 094505.

[25] J. B. Kogut, M. A. Stephanov, D. Toublan, J. J. M. Verbaarschot, A. Zhitnitsky, Nucl. Phys. B582 (2000) 477.

[26] R. Aloisio, V. Azcoiti, G. Di Carlo, A. Galante, A. F. Grillo, Nucl. Phys. B606 (2001) 322.

[27] S. Muroya, A. Nakamura, C. Nonaka, Prog. Theor. Phys. Suppl. 153 (2004) 51.

[28] S. Muroya, A. Nakamura, C. Nonaka, Phys. Lett. B551 (2003) 305.

[29] M. P. Lombardo, M. L. Paciello, S. Petrarca, B. Taglienti, Nucl. Phys. (Proc. Suppl.) 129 (2004) 635; work in progress.

[30] F. Sannino, Phys. Rev. D67 (2003) 054006.

[31] M. A. Metlitski, A. R. Zhitnitsky, hep–ph/0508004.

[32] G. 't Hooft, Phys. Rept. 142 (1986) 357.

[33] R. Rapp, T. Schäfer, E. V. Shuryak, M. Velkovsky, Phys. Rev. Lett. 81 (1998) 53.

[34] A. R. Zhitnitsky, hep–ph/0601057.

[35] J. B. Kogut, L. Susskind, Phys. Rev. D11 (1975) 395.

[36] H. Kluberg–Stern, A. Morel, O. Napoly, B. Petersson, Nucl. Phys. B220 (1983) 447.

[37] P. Hasenfratz, F. Karsch, Phys. Lett. B125 (1983) 308; J. B. Kogut et al., Nucl. Phys. B225 (1983) 93.

[38] K. G. Wilson, Phys. Rev. D10 (1974) 2445.

[39] S. Duane, J. B. Kogut, Nucl. Phys. B275 (1986) 398.

[40] S. Gottlieb et al., Phys. Rev. D35 (1987) 2531; O. Martin, S. W. Otto, Phys. Rev. D31 (1985) 435.

[41] B. Allés, G. Boyd, M. D'Elia, A. Di Giacomo, E. Vicari, Phys. Lett. B389 (1996) 107.

[42] B. Allés et al., Phys. Rev. D58 (1998) 071503.

[43] Y. Aoki et al., hep–lat/0411006.

[44] J. B. Kogut, D. Toublan, D. K. Sinclair, Nucl. Phys. B642 (2002) 181.

[45] M. Campostrini, A. Di Giacomo, H. Panagopoulos, E. Vicari, Nucl. Phys. B329 (1990) 683.

[46] P. H. Ginsparg, K. G. Wilson, Phys. Rev. D25 (1982) 2649.

[47] H. Neuberger, Phys. Lett. B417 (1998) 141; M. Lüscher, Phys. Lett. B428 (1998) 342.

[48] L. Giusti, G. C. Rossi, M. Testa, Phys. Lett. B587 (2004) 157.

[49] M. Campostrini, A. Di Giacomo, H. Panagopoulos, Phys. Lett. B212 (1988) 206.

[50] B. Allés, E. Vicari, Phys. Lett. B268 (1991) 241.

[51] D. Espriu, R. Tarrach, Z. Phys. C16 (1982) 77.

[52] B. Allés, A. Di Giacomo, H. Panagopoulos, E. Vicari, Phys. Lett. B350 (1995) 70.

[53] W. Zimmermann in "Lectures on Elementary Particles and Quantum Field Theory", 1970 Brandeis School, edited by S. Deser, M. Grisaru, H. Pendleton.

[54] E. Seiler, I. O. Stamatescu, preprint MPI–PAE/PTh 10/87 (1987), unpublished.

[55] K. Osterwalder in "Constructive Field Theory", Lecture Notes in Physics, n° 25, 1973, edited by G. Velo, A. S. Wightman.

[56] P. Menotti, A. Pelissetto, Nucl. Phys. B (Proc. Suppl.) 4 (1988) 644.

[57] B. Allés, M. D'Elia, A. Di Giacomo, R. Kirchner, Phys. Rev. D58 (1998) 114506.

[58] I. Horváth et al., Phys. Lett. B617 (2005) 49.

[59] E.–M. Ilgenfritz, K. Koller, Y. Koma, G. Schierholz, T. Streuer, V. Weinberg, hep–lat/0512005.

[60] A. Di Giacomo, E. Vicari, Phys. Lett. B275 (1992) 419.

[61] B. Allés, M. Campostrini, A. Di Giacomo, Y. Gündüç, E. Vicari, Phys. Rev. D48 (1993) 2284.

[62] M. D'Elia, Nucl. Phys. B661 (2003) 139.

[63] M. Teper, Phys. Lett. B171 (1986) 81; Phys. Lett. B171 (1986) 86.

[64] B. Allés, L. Cosmai, M. D'Elia, A. Papa, Phys. Rev. D62 (2000) 094507.

[65] B. Allés, M. D'Elia, A. Di Giacomo, C. Pica, Proc. Sci. (LAT2005) 316, (hep–lat/0509024); hep–lat/0604007.

[66] P. Di Vecchia, K. Fabricius, G. C. Rossi, G. Veneziano, Nucl. Phys. B192 (1981) 392; Phys. Lett. B108 (1982) 323.

[67] C. Christou, A. Di Giacomo, H. Panagopoulos, E. Vicari, Phys. Rev. D53 (1996) 2619.

[68] W. Pauli, Nuovo Cimento 6 (1957) 205; F. Gürsey, Nuovo Cimento 7 (1958) 411.

[69] W. H. Press, S. A. Teukolsky, W. T. Vetterling, B. P. Flannery, "Numerical Recipes in Fortran 77", 2nd edition (1992), Cambridge University Press.

[70] B. Allés, M. D'Elia, work in progress.

[71] D. Toublan, A. R. Zhitnitsky, hep–ph/0503256.

[72] J. I. Skullerud, S. Hands, S. Kim, hep–lat/0511001.